International Journal of Minerals, Metallurgy and Materials
Volume 25, Number 9, September 2018, Page 1027
https://doi.org/10.1007/s12613-018-1653-0

Direct electrodeposition of ionic liquid-based template-free SnCo alloy nanowires as an anode for Li-ion batteries

Le-ping Wang[1)], *Gang Chen*[1)], *Qi-xin Shen*[1)], *Guo-min Li*[1)], *Shi-you Guan*[2)], *and Bing Li*[1)]

1) School of Materials science and Engineering, East China University of Science and Technology, Shanghai 200237, China

2) Institute for Sustainable Energy, Shanghai University, Shanghai 200444, China

(Received: 11 January 2018; revised: 16 April 2018; accepted: 19 April 2018)

Abstract: SnCo alloy nanowires were successfully electrodeposited from $SnCl_2$–$CoCl_2$–1-ethyl-3-methylimidazolium chloride (EMIC) ionic liquid without a template. The nanowires were obtained from the molar ratio of 5:40:60 for $SnCl_2$:$CoCl_2$:EMIC at −0.55 V and showed a minimum diameter of about 50 nm and lengths of over 20 μm. The as-fabricated SnCo nanowires were about 70 nm in diameter and featured a Sn/Co weight ratio of 3.85:1, when used as an anode for a Li-ion battery, they presented respective specific capacities of 687 and 678 $mAh·g^{-1}$ after the first charge and discharge cycle and maintained capacities of about 654 $mAh·g^{-1}$ after 60 cycles and 539 $mAh·g^{-1}$ after 80 cycles at a current density of 300 $mA·g^{-1}$. Both the nanowire structure and presence of elemental Co helped buffer large volume changes in the Sn anode during charging and discharging to a certain extent, thereby improving the cycling performance of the Sn anode.

Keywords: SnCo alloy; nanowires; template; electrodeposition; ionic liquid

1. Introduction

The graphite anode in current Li-ion batteries has shown the disadvantages of a relatively low capacity (theoretical specific capacity, 372 $mAh·g^{-1}$) and potential safety issues [1–2]. Metal-based anode materials, such as Sn-based alloys, are regarded as possible alternative anodes for these batteries because such materials feature a higher specific capacity (993 $mAh·g^{-1}$) and better safety than their graphite counterparts [3]. However, Sn-based alloys also exhibit significant and irreversible capacity degradation due to serious volume expansion in the charge and discharge processes [4]. Both alloying and nano-structured Sn-based anodes are expected to solve these problems. Addition of alloying elements to Sn-based alloys, such as the transition metal elements Fe, Co, and Ni, can provide barriers to effectively relieve the volume change of Sn-based anodes during charging and discharging [5–8].

Electrodeposition is a relatively simple and inexpensive method to prepare alloys. Hassoun *et al.* [9] reported that Sn–Ni alloy films electrodeposited on Cu foil show a capacity of 550 $mAh·g^{-1}$ after 40 cycles. Tamura *et al.* [10] electrodeposited an amorphous SnCo alloy film with a rough surface that showed a specific capacity of 600 $mAh·g^{-1}$ after 20 cycles. Wang *et al.* [11] successfully synthesized core-shell Cu–Sn alloys on a Cu nanowire array current collector, this device featured a specific capacity 552 $mAh·g^{-1}$ after 60 cycles when used as an anode for Li-ion batteries.

Compared with general particle-based electrodes, nanowire-based electrodes allow more space with which to buffer volume expansion of the electrode in Li-ion batteries [12]. Templates are generally required to prepare nanowires during electrodeposition of alloys. For example, Ferrara *et al.* [13] electrochemically synthesized SnCo alloy nanowires by using a polycarbonate-membrane template. Tian *et al.* [14] prepared a NiSn nanowire anode by electrodeposition with a porous anodic alumina template, and the resulting anode gave a capacity of about 250 $mAh·g^{-1}$ after 60 cycles. Despite its many benefits, however, template-assisted electrodeposition is a very complicated and tedious process because the template must be prepared before the experiment and dissolved after the experiment. As such, exploration of a template-free electrodeposition method to

Corresponding author: Bing Li E-mail: bingli@ecust.edu.cn; Guan-shi You E-mail: syguan@ecust.edu.cn

obtain Sn-based alloy nanowires is a meaningful endeavor.

Ionic liquids are a type of liquid salt at close to room temperature. As they generally feature lower conductivity (10^{-6}–10^{-5} S·m^{-1}) compared with aqueous solution (0.5 × 10^{-3}–15 × 10^{-3} S·m^{-1}) and higher viscosity compared with aqueous solutions, suitable media to produce nanowires in ionic liquid without template could be developed. In fact, Al, Te, and SmCo nanowires have been obtained from $AlCl_3$-trimethylamine hydrochloride (TMHC), a piperidinium-based mixed ionic liquid, and $SmCl_3$–$CoCl_2$–1-ethyl-3-methylimidazolium chloride (EMIC) ionic liquid, respectively, via a template-free electrodeposition method according to the literature and our previous work [15–17]. Chen *et al.* [18] electrodeposited AlFe alloy nanowires from TMHC–$AlCl_3$–$FeCl_3$ ionic liquid without a template. Hsieh and Sun [19] successfully prepared CuSn nanobrushes from 1-ethyl-3-methylimidazolium dicyanamide ionic liquid at a current density of −0.4 mA·cm^{-2}. The slow ion diffusion rate of the ionic liquid and an appropriate electrodeposition potential are key factors for preparation electrodepositing nanowires without a template.

Based on our previous work on the template-free electrodeposition of SmCo nanowires from $SmCl_3$–$CoCl_2$–EMIC ionic liquid, herein, we electrodeposited SnCo alloy nanowires from $SnCl_2$–$CoCl_2$–EMIC ionic liquid without a template. The as-prepared SnCo alloy nanowires were used as an anode for a Li-ion battery, and they exhibited outstanding cyclic performance and specific capacities of about 760 mAh·g^{-1} after the first cycle, 600 mAh·g^{-1} after 60 cycles, and 408 mAh·g^{-1} after 80 cycles at a current density of 300 mA·g^{-1}.

2. Experimental

The raw materials, including EMIC (ACROS, 97wt%), $CoCl_2$, and $SnCl_2$ (Alfa Aesar, 99.9wt%) were bought and directly used without any treatments. The ionic liquid was prepared by adding EMIC, $CoCl_2$, and $SnCl_2$ into a beaker at a specific molar ratio and then heating to a given temperature for 2 h with continuous stirring in an Ar-filled glove box. A three-electrode system was applied for all electrochemical analyses and electrodeposition experiments; here, W wire (99wt%) and a Cu sheet served as the working electrode for voltammetric studies and electrodeposition, respectively, and a Co plate (Aladdin, 99.5wt%) served as the counter electrode. The reference electrode was prepared by immersing a Co wire (Aladdin, 99.5wt%) into a 40:60 molar ratio of $CoCl_2$–EMIC ionic liquid in a fritted glass tube as referenced in our previous work [17]. In the experiments, all potentials are reported relative to the above reference electrode. A PAR-STAT2273 (PAR-Ametek Co., Ltd.) workstation with the PowerSUITEuite software package was used to record all electrochemical and electrodeposition data. The W wire (99wt%), Cu sheet, and Co plate were polished with emery papers, washed with distilled water and acetonitrile, and then dried in a vacuum oven before use. After each electrodeposition experiment, the SnCo alloy deposits that formed on the Cu sheet were quickly moved to acetonitrile and cleaned three times. Thereafter, they were directly assembled into a coin-type cell with a Li plate (ϕ16 mm × 1.5 mm, China Energy Lithium Co., Ltd.) in 1 mol·L^{-1} $LiPF_6$ with ethylene carbonate, dimethyl carbonate, and ethyl methyl carbonate (1:1:1 in volume ratio) electrolyte and a Celgard 2400 separator.

Electrochemical analysis and electrodeposition were conducted inside an Ar-filled glove box in which the concentration of O_2 and H_2O are less than 1 mg/L. Scanning electron microscopy (SEM, JEOLJSM-6360LV), transmission electron microscopy, and high-resolution transmission electron microscopy (TEM/HRTEM, JEM-2100, 200 kV) were employed to characterize the morphology of the deposits. An energy dispersive X-ray spectroscope (EDS, Falcon) and inductively coupled plasma atomic emission spectrometer (ICP, Agilent) were used to analyze the chemical composition of the deposits. Selected area electron diffraction (SAED, JEM-2100, 200 kV) was employed to analyze the structure of deposits, and a charge/discharge battery tester (NewWare TC5.X, Shenzhen) was used to test the performance of the battery at cut-off voltages between 0.01 and 1.5 V vs. Li/Li$^+$.

3. Results and discussion

3.1. Electrochemical reduction of Co^{2+} and Sn^{2+} ions in $SnCl_2$–$CoCl_2$–EMIC ionic liquid

Fig. 1 shows cyclic voltammograms (CVs) recorded on W electrodes in $CoCl_2$–EMIC ionic liquid with or without $SnCl_2$. In curve 1 of Fig. 1, the reduction peak A and the oxidation peak B are attributed to Co^{2+} reduction and Co

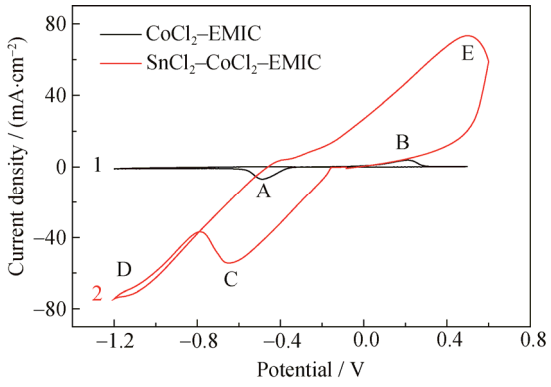

Fig. 1. Cyclic voltammograms recorded on a W electrode in $SnCl_2$–$CoCl_2$–EMIC ionic liquid (0:40:60, 5:40:60 in molar ratio) at 120°C and scan rate of 50 mV·s^{-1}.

oxidation in the ionic liquid. As $SnCl_2$ is added to the $CoCl_2$–EMIC ionic liquid (40:60 in molar ratio), i.e., $SnCl_2$–$CoCl_2$–EMIC (5:40:60 in molar ratio), reduction peaks C and D, as well as oxidation peak E, are shown in curve 2 of Fig. 1. The reduction peak C at −0.6 V corresponds to co-reduction of Co^{2+} and Sn^{2+}; Co reduction, which begins at about −0.15 V, is proven by the following electrodeposition study. The reduction peak D at −1.1 V is related to Sn reduction. Apparently, addition of $SnCl_2$ to $CoCl_2$–EMIC ionic liquid causes a much higher reduction current density.

3.2. Electrodeposition of Co nanowires

According to our previous work [17], Co nanowires were obtained by electrodeposition from $CoCl_2$–EMIC ionic liquid with a molar ratio of 40:60 at −0.65 V and 120°C for 1200 s and from the same liquid with a molar ratio of 60:60 at −0.68 V and 90°C for 1200 s. The Co nanowire diameters obtained were in the range of about 450–530 nm. The formation mechanism of Co nanowires can be explained according to Fig. 2. The electrical double layer is first charged as soon as a reduction potential of over −0.2 V is imposed on the working electrode. Then, Co^{2+} ions are reduced onto the Cu substrate, and new Co nuclei are formed followed by their growth. Initially, Co^{2+} ions shift to the cathode (Cu substrate) driven by the electric field force and are consumed by electrochemical reduction, during which a concentration gradient of Co^{2+} ions is built between the Cu electrode and the bulk or between Co nuclei and the ionic liquid around these nuclei. Then, Co^{2+} ions migrate to the cathode under both the electric field force and the concentration gradient, as shown in Fig. 2(a); in this figure, F_1 refers to the electric field force and F_2 refers to the force caused by the Co^{2+} ion concentration gradient. As electrodeposition proceeds, Co nuclei continuously grow along the perpendicular and parallel directions relative to the cathode substrate. As Co^{2+} ions around the formed Co nuclei are completely consumed, Co^{2+} ions diffuse from the bulk ionic liquid to the top of the formed Co nuclei for further electrodeposition, leading to vertical Co nuclear growth relative to the cathode Cu substrate. Co nuclear growth parallel to the cathode substrate is limited at this point by the extremely slow diffusion rate of Co^{2+} in the ionic liquid. Co nanowires with a certain length diameter ratio are finally obtained after several cycles of this process, as presented in Fig. 2(b).

3.3. Electrodeposition of SnCo alloy

SnCo alloys were prepared from $SnCl_2$–$CoCl_2$–EMIC ionic liquid using the specific experimental conditions listed in Table 1. All Sn/Co weight ratios were obtained by ICP analyses. In $SnCl_2$–$CoCl_2$–EMIC ionic liquid with a molar ratio of 5:40:60 at 120°C for 300 s, the deposits with Sn/Co weight ratios of about 3.41:1, 3.85:1, 5.14:1, 4.81:1, and 5:1 are obtained at applied potential changes of −0.45, −0.5, −0.55, −0.58, and −0.6 V, respectively. The SnCo alloy shows a leaf-like morphology measuring about 300 nm in size at −0.45 V (Fig. 3(a)). As the potential is shifted to −0.5 V

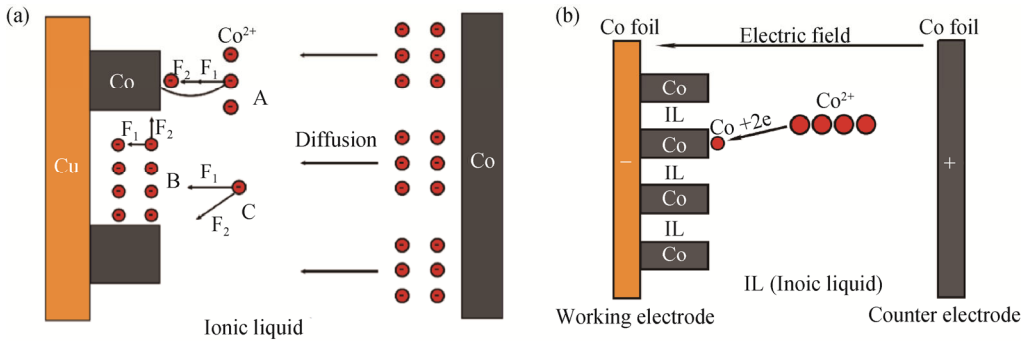

Fig. 2. Schematic of (a) Co^{2+} ions migration to the cathode under both the electric field force and the concentration gradient and (b) formation process of Co nanowires in $CoCl_2$–EMIC ionic liquid (40:60 in molar ratio).

Table 1. Electrodeposition conditions for obtaining SnCo alloy

Samples	Potential / V	Time and temperature	Morphology	Diameter / nm	Length / μm	Sn:Co (in wt%)
SnCo5-0.45	−0.45	300 s, 120°C	Leaf-like	≈300	—	3.41:1
SnCo5-0.5	−0.50		Nanowires	70	>20	3.85:1
SnCo5-0.55	−0.55		Nanowires	50	>>20	5.14:1
SnCo5-0.58	−0.58		Flower-like	≈550	—	4.81:1
SnCo5-0.6	−0.60		Sunflower-like	≈300	—	5:1
SnCo8-0.55	−0.55		Fishbone-like	≈220	≈20	5.6:1

Notes: In samples labeled SnCoX-Y, X indicates the $SnCl_2$ content in $SnCl_2$–$CoCl_2$–EMIC and Y indicates the applied potential during electrodeposition.

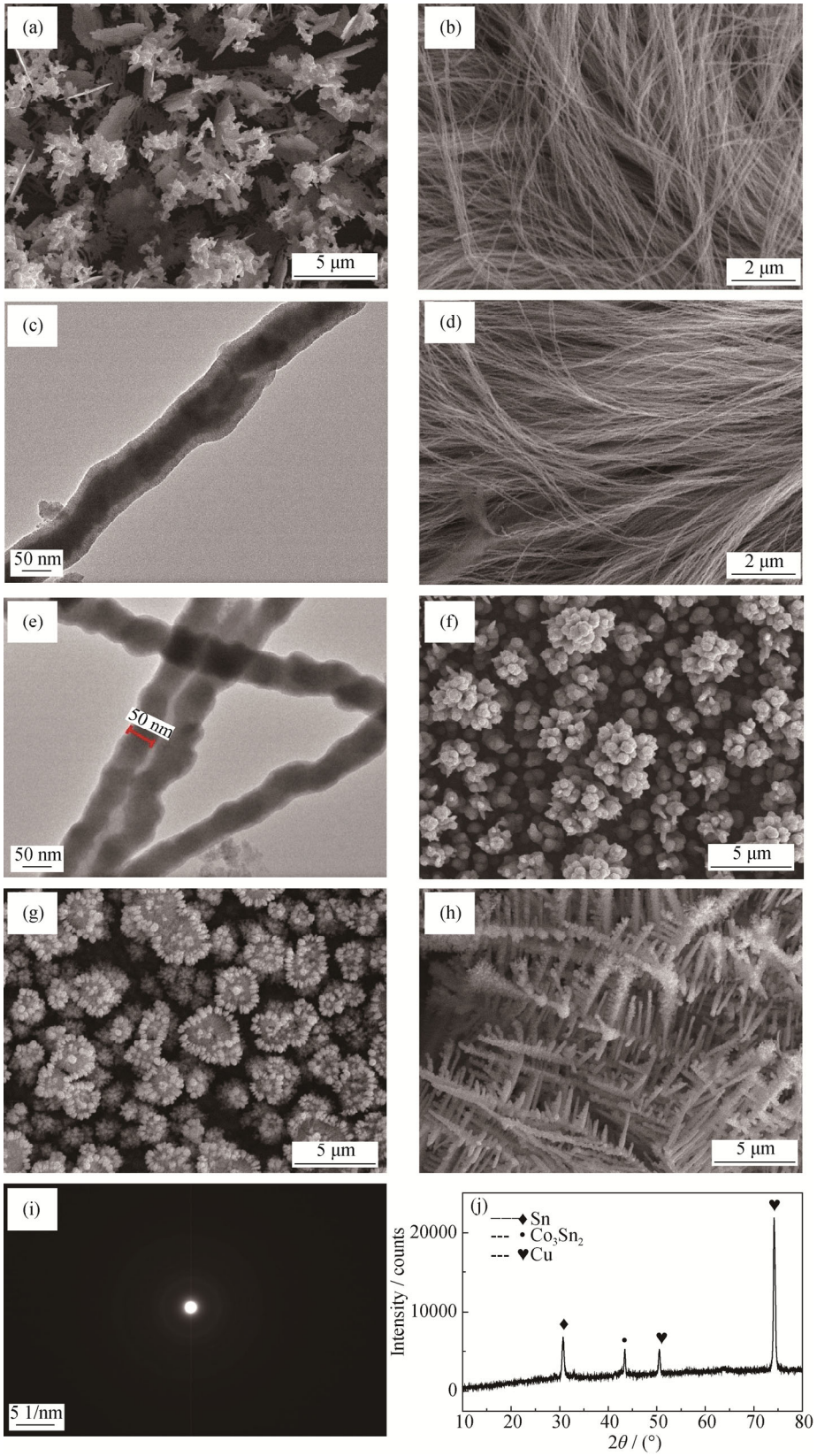

Fig. 3. Surface morphologies, SAED image and XRD pattern of the SnCo alloys from $SnCl_2$−$CoCl_2$−EMIC ionic liquid with 5:40:60 in molar ratio or with 8:40:60 in molar ratio at 120°C, 300 s: (a) SEM of the SnCo5-0.45 alloys; (b) SEM of the SnCo5-0.5 alloys; (c) TEM image of (b); (d) SEM of the SnCo5-0.55 alloys ; (e) TEM image of (d); (f) SEM of the SnCo5-0.58 alloys; (g) SEM of the SnCo5-0.6 alloys; (h) SEM of the SnCo8-0.55 alloys; (i) SAED image of SnCo5-0.55; (j) XRD pattern of SnCo5-0.55.

in the same ionic liquid, SnCo nanowires with an average diameter of about 70 nm and lengths of over 20 μm are gained, as shown in Figs. 3(b) and 3(c). Addition of a small amount of $SnCl_2$ to the $CoCl_2$–EMIC ionic liquid does not disrupt the conditions required to form the nanowires and can effectively reduce the nanowire diameter from 450 nm to 70 nm, as seen in the TEM image in Fig. 3(c). As the potential further decreases to −0.55 V, the as-prepared SnCo nanowires present an average diameter of about 50 nm, as seen in Fig. 3(d), slightly thinner than that obtained at −0.5 V. The TEM image in Fig. 3(e) reveals that the average length of the SnCo nanowires is much longer than 20 μm. Thus, more negative potentials clearly produce thinner nanowires with higher weight ratios of Sn/Co. As the potential is adjusted to −0.58 V, a completely different appearance of SnCo is achieved from the same ionic liquid, and the deposits are notably composed of powders rather than nanowires (Fig. 3(f)). Some powders even accumulate together to form a flower-like structure. The average size of these powders is about 500–600 nm. As the potential is decreased to −0.6 V, the sunflower-like deposits in Fig. 3(g) are obtained; the sample obtained at this point consists of short nanowires in the root portion and powders in the top portion, and the weight ratio of Sn/Co in the deposits is about 5:1. As the composition of $SnCl_2$–$CoCl_2$–EMIC is changed to 8:40:60 in molar ratio, the as-prepared SnCo alloy obtained at −0.55 V resembles fishbones with a diameter of about 220 nm (Fig. 3(h)); here, the weight ratio of Sn/Co is about 5.6:1. SAED image analysis indicates that the pure Co nanowires feature a completely amorphous structure without any diffraction rings [17]. By contrast, the SnCo nanowires in Fig. 3(i) reveal a mainly amorphous structure with some obvious diffraction rings. This result shows that the crystal quality of the SnCo nanowires is improved by addition of $SnCl_2$. The presence of Sn and Co_3Sn_2 alloy in the SnCo nanowires is confirmed by the XRD pattern shown in Fig. 3(j); here, peaks at 2θ of 30.644° and 43.528° correspond to Sn and Co_3Sn_2, respectively. The highest peaks at 2θ of 74.13° and 50.433° reflect the Cu sheet substrate.

3.4. Electrochemical performances of the SnCo nanowires

The effects of morphology and SnCo nanowire composition on the electrochemical performance of the anodes used in a Li-ion battery were investigated. Here, capacity is calculated for the total mass of the SnCo alloy, which is about 0.5–1 mg and measured by an analytical balance. As detailed in Table 1, the samples are designated SnCoX-Y, where X and Y represent the $SnCl_2$ molar ratio in the ionic liquid and the potential applied during electrodeposition, respectively. First, all of the batteries were charged and discharged for one cycle at a current density of 100 $mA{\cdot}g^{-1}$ to stabilize the anode material prior to formal charge and discharge studies. Fig. 4 shows the CVs of the SnCo5-0.55 nanowire anode (in a SnCo–Li coin battery). The two pairs of reduction (peaks A, B) and oxidation (peaks C, D) peaks in Fig. 4 correspond to the two intercalation/deintercalation platforms in Fig. 5(a), where the reduction peaks A and B at around 0.33 and 0.12 V, respectively are derived from the different Li intercalation processes of Li_xSn, as described in Eqs. (1) and (2) [20–22]. In the oxidation process shown in Fig. 5(a), the two anode peaks C and D at 0.56 and 0.68 V, respectively, reflect Li-ion deintercalation from the Li–Sn alloy.

$$\frac{1}{x}CoSn_x + xLi^+ + xe^- \rightarrow \frac{1}{x}Co + Li_xSn \quad (1)$$

$$Li_xSn \leftrightarrow xLi^+ + xe^- + Sn \quad (2)$$

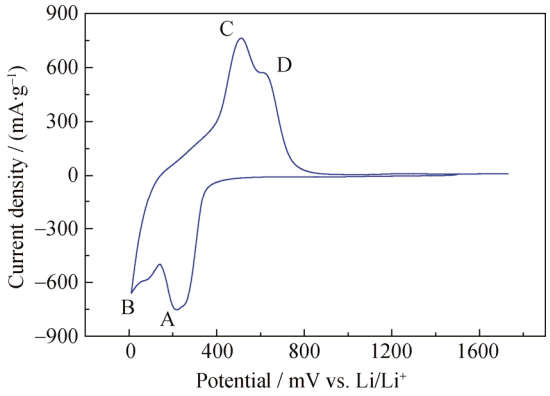

Fig. 4. Cyclic voltammograms of the SnCo5-0.55 nanowire anode (in a SnCo–Li coin battery) at 0.1 $mV{\cdot}s^{-1}$.

SnCo5-0.5 shows relatively good cycling ability at a charge–discharge current of 300 $mA{\cdot}g^{-1}$ in Fig. 5(a); in this figure, the SnCo nanowires appear to present two potential platforms. The SnCo5-0.55 anode in Fig. 5(b) delivers specific capacities of about 765 and 760 $mAh{\cdot}g^{-1}$ during the first charge and discharge cycle. This capacity is maintained at about 600 $mAh{\cdot}g^{-1}$ for 60 cycles, after which the discharge capacity is reduced to about 408 $mAh{\cdot}g^{-1}$ after 80 cycles. During the charge–discharge process, the average coulombic efficiency of the SnCo nanowires is about 97%.

SnCo5-0.5 shows specific capacities of 687 and 678 $mAh{\cdot}g^{-1}$ for the first charge and discharge process at a current density of 300 $mA{\cdot}g^{-1}$, as shown in Fig. 5(b). Its capacity is then maintained about 654 $mAh{\cdot}g^{-1}$ after 60 cycles and 539 $mAh{\cdot}g^{-1}$ after 80 cycles. The average coulombic efficiency of this anode is also as high as 96%. In Fig. 5(b), the

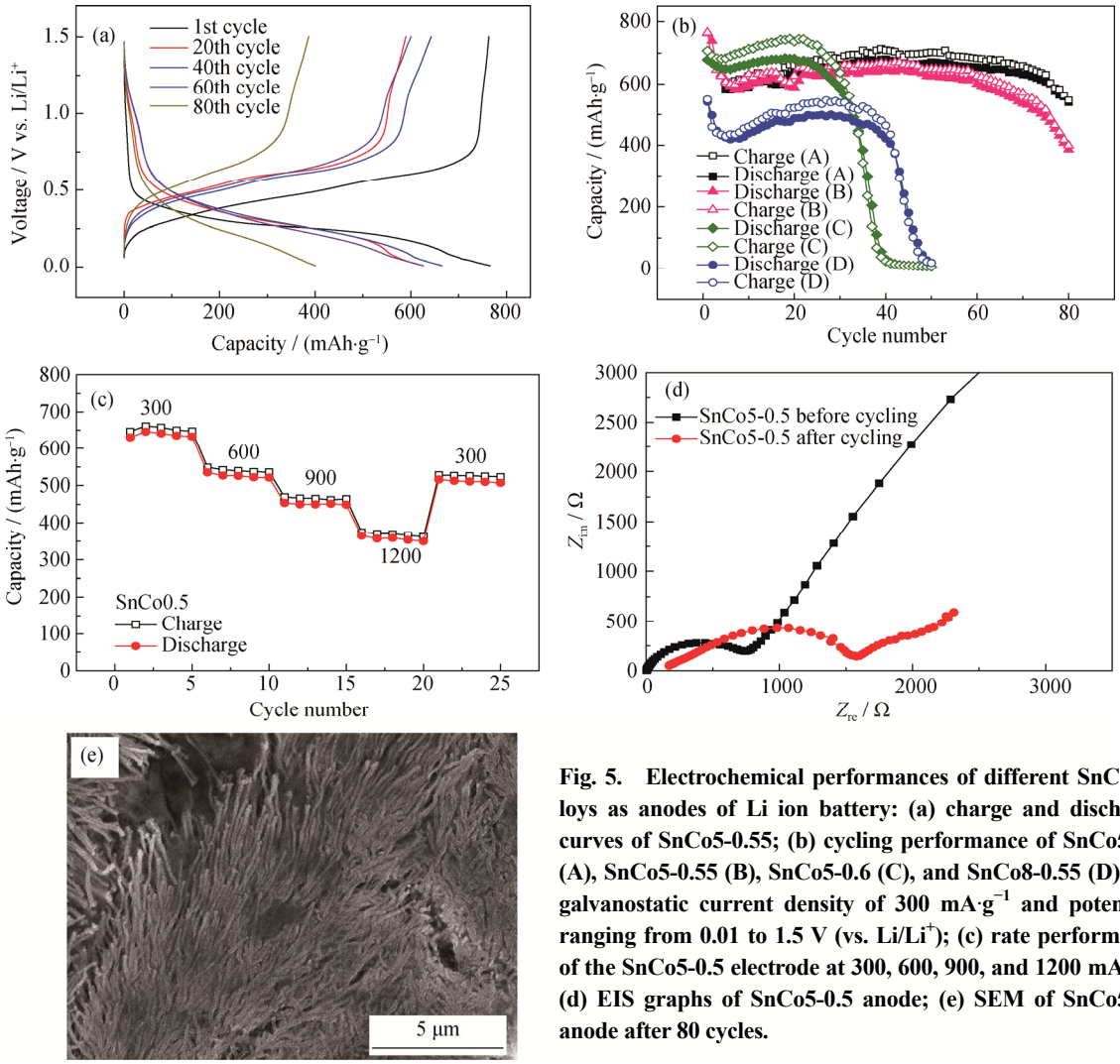

Fig. 5. Electrochemical performances of different SnCo alloys as anodes of Li ion battery: (a) charge and discharge curves of SnCo5-0.55; (b) cycling performance of SnCo5-0.5 (A), SnCo5-0.55 (B), SnCo5-0.6 (C), and SnCo8-0.55 (D) at a galvanostatic current density of 300 mA·g^{-1} and potentials ranging from 0.01 to 1.5 V (vs. Li/Li$^+$); (c) rate performance of the SnCo5-0.5 electrode at 300, 600, 900, and 1200 mA·g^{-1}; (d) EIS graphs of SnCo5-0.5 anode; (e) SEM of SnCo5-0.5 anode after 80 cycles.

SnCo alloy clearly provides a relatively smaller capacity at −0.5 V than that at −0.55 V in the first 10 cycles, but the lower content of elemental Sn in the SnCo5-0.5 nanowires makes these wires more stable than other samples during the following charge–discharge cycles. Therefore, elemental Co is quite useful for easing large volume changes in Sn during Li-ion intercalation and deintercalation. Among the samples, SnCo5-0.6 presents the highest capacity of about 700 mAh·g^{-1} in the first cycle because of the significant amount of Sn in the alloy, as seen in Fig. 5(b). However, the capacity of this sample is rapidly reduced to about 0 mAh·g^{-1} after 40 cycles, indicating poor cycling ability. This degradation of capacity may be attributed to the large particle size of the alloy. SnCo8-0.55 shows a discharge capacity of 560 mAh·g^{-1} at the first cycle and about 0 mAh·g^{-1} after 50 cycles, as seen in Fig. 5(b). The high Sn content of SnCo8-0.55 changes the morphology of the alloy from nanowires to fishbones, which brings about larger volume changes during the charge–discharge process. Comparison of the cycling performances of SnCo5-0.5, SnCo5-0.55, SnCo5-0.6, and SnCo8-0.55 reveals that the SnCo5-0.5 nanowires (prepared from 5:40:60 in molar ratio ionic liquid at −0.5 V and 120°C for 300 s) present the highest capacity and the best cyclability because of their small diameter and the suitable molar ratio of Sn and Co elements in the alloy. Fig. 5(c) illustrates the rate performance of the SnCo5-0.5 electrode. Here at current densities of 300, 600, 900, and 1200 mA·g^{-1}, the electrode exhibits steady and reversible specific charge capacities of 647, 549, 470, and 375 mAh·g^{-1}, respectively. In addition, the capacity decreases to 528 mAh·g^{-1} when the current density is returned to the initial value of 300 mA·g^{-1}. The electrochemical impedance spectra (EIS) of the SnCo5-0.5 anode before and after cycling reveal that its contact resistance increases from 4 ohms to 170 ohms and its charge transfer resistance increases from 750 ohms to 1450 ohms after 80 cycles, as shown in

Fig. 5(d). SnCo5-0.5 maintains its nanowire-like morphology but the wires acquire a larger diameter than that of the initial sample after 80 cycles, as shown in Fig. 5(e). The nanowire structure facilitates improvements in cycling ability, and addition of a certain amount of Co to the SnCo alloy nanowire is necessary to overcome volume changes during Li ion intercalation and deintercalation. Further reductions in the size of the SnCo nanowires or addition of other elements may be necessary to improve the cycling ability of the SnCo alloys.

4. Conclusions

SnCo alloy nanowires were successfully electrodeposited from $SnCl_2$–$CoCl_2$–EMIC ionic liquid at a constant potential without a template. The average diameter of the SnCo alloy nanowires obtained in 5:40:60 in molar ratio $SnCl_2$–$CoCl_2$–EMIC at −0.55 V was about 50 nm, which means these nanowires are much finer than pure Co nanowires, which feature an average diameter about 450 nm. The SnCo alloy nanowire electrode exhibited good performance with a relatively high specific capacity. The results showed that the nanowire arrays are able to accommodate large volume changes caused by Li ion intercalation and deintercalation. The fabricated SnCo nanowire electrodes (70 nm in diameter, Sn:Co weight ratio of 3.85:1) exhibited specific capacities of 687 and 678 $mAh \cdot g^{-1}$ during the first charge and discharge cycle and maintained capacities of about 654 $mAh \cdot g^{-1}$ after 60 cycles and 539 $mAh \cdot g^{-1}$ after 80 cycles at a current density of 300 $mA \cdot g^{-1}$. Both the fineness of the nanowires and the presence of the transition metal Co could buffer large volume changes during Li ion intercalation and deintercalation, thereby improving the cycling performance of the Sn anode.

Acknowledgements

This work was financially supported by the National Natural Science Foundation of China (No. 51474107) and the Opening Project Fund of Key Laboratory of Common Associated Non-ferrous Metal Resources Pressure Hydrometallurgy Technology (No. yy2016008).

References

[1] J.M. Tarascon and M. Armand, Issues and challenges facing rechargeable lithium batteries, *Nature*, 414(2001), p. 359.

[2] T. Li, J.Y. Yang, and S.G. Lu, Effect of modified elastomeric binders on the electrochemical properties of silicon anodes for lithium-ion batteries, *Int. J. Miner. Metall. Mater.*, 19(2012), No. 8, p. 752.

[3] T. Huang, Y. Yao, Z. Wei, Z. Liu, and A.S. Yu, Sn-Co-artificial graphite composite as anode material for rechargeable lithium batteries, *Electrochim. Acta*, 56(2010), No. 1, p. 476.

[4] R. Yang, J. Huang, W. Zhao, W.Z. Lai, X.Z. Zhang, J. Zheng, and X.G. Li, Bubble assisted synthesis of Sn–Sb–Cu alloy hollow nanostructures and their improved lithium storage properties, *J. Power Sources*, 195(2010), No. 19, p. 6811.

[5] M.J. Lindsay, G.X. Wang, and H.K. Liu, Al-based anode materials for Li-ion batteries, *J. Power Sources*, 119(2003), p. 84.

[6] T. Huang, Y. Yao, Z. Wei, Z. Liu, and A.S. Yu, Sn–Co–artificial graphite composite as anode material for rechargeable lithium batteries, *Electrochim. Acta*, 56(2010), No. 1, p. 476.

[7] D.H. Nam, R.H. Kim, C.L. Lee, and H. Kwon, Highly reversible Sn–Co alloy anode using porous Cu foam substrate for Li-ion batteries, *J. Electrochem. Soc*., 159(2012), No. 11, p. A1822.

[8] J. Hassoun, S. Panero, G. Mulas, and B. Scrosati. An electrochemical investigation of a Sn–Co–C ternary alloy as a negative electrode in Li-ion batteries, *J. Power Sources*, 171(2007), No. 2, p. 928.

[9] J. Hassoun, S. Panero, P. Simon, P.L. Taberna, and B. Scrosati, High-rate, long-life Ni–Sn nanostructured electrodes for lithium-ion batteries, *Adv. Mater.*, 19(2007), No. 12, p. 1632.

[10] N. Tamura, M. Fujimoto, M. Kamino, and S. Fujitani, Mechanical stability of Sn–Co alloy anodes for lithium secondary batteries, *Electrochim. Acta*, 49(2004), No. 12, p. 1949.

[11] J.Z. Wang, N. Du, H. Zhang, J.X. Yu, and D.R. Yang, Cu–Sn core-shell nanowires arrays as three-dimensional electrodes for lithium-ion batteries, *J. Phys. Chem. C*, 115(2011), No. 47, p. 23620.

[12] J. Yi, Y.L. Liu, Y. Wang, X.P. Li, S.J. Hu, and W.S. Li, Synthesis of dandelion-like TiO_2 microspheres as anode materials for lithium ion batteries with enhanced rate capacity and cyclic performances, *Int. J. Miner. Metall. Mater.*, 19(2012), No. 11, p. 1058.

[13] G. Ferrara, L. Damen, C. Arbizzani, R. Inguanta, S. Piazza, C. Sunseri, and M. Mastragostino, SnCo nanowire array as negative electrode for lithium-ion batteries, *J. Power Sources*, 196(2011), No. 3, p. 1469.

[14] M. Tian, W. Wang, S.H. Lee, Y.C. Lee, and R.G. Yang, Enhancing Ni–Sn nanowire lithium-ion anode performance by tailoring active/inactive material interfaces, *J. Power Sources*, 196(2011), No. 23, p. 10207.

[15] C.J. Su, Y.T. Hsieh, C.C. Chen, and I.W. Sun, Electrodeposition of aluminum wires from the Lewis acidic $AlCl_3$/trimethylamine hydrochloride ionic liquid without using a template, *Electrochem. Commun.*, 34(2013), p. 170.

[16] J. Szymczak, S. Legeai, S. Diliberto, S. Migot, N. Stein, C.

Boulanger, G. Chatel, and M. Draye, Template-free electrodeposition of tellurium nanostructures in a room-temperature ionic liquid, *Electrochem. Commun*., 24(2012), p. 57.

[17] Y.Q. Chen, H. Wang, and B. Li, Electrodeposition of SmCo alloy nanowires with a large length-diameter ratio from $SmCl_3$–$CoCl_2$–1-ethyl-3-methylimidazolium chloride ionic liquid without template, *RSC Adv*., 5(2015), No. 49, p. 39620.

[18] G. Chen, Y.Q. Chen, Q.J. Guo, H. Wang, and B. Li, Template-free electrodeposition of AlFe alloy nanowires from a room-temperature ionic liquid as an anode material for Li-ion batteries, *Faraday Discuss.*, 190(2016), p. 97.

[19] Y.T. Hsieh and I.W. Sun, Electrochemical growth of hierarchical CuSn nanobrushes from an ionic liquid, *Electrochem. Commun.*, 13(2011), No. 12, p. 1510.

[20] S.I. Lee, S. Yoon, C.M. Park, J.M. Lee, H. Kim, D. Im, S.G. Doo, and H.J. Sohn, Reaction mechanism and electrochemical characterization of a Sn–Co–C composite anode for Li-ion batteries, *Electrochim. Acta*, 54(2009), No. 2, p. 364.

[21] J.C. He, H.L. Zhao, M.W. Wang, and X.D. Jia, Preparation and characterization of Co–Sn–C anodes for lithium-ion batteries, *Mater. Sci. Eng. B,* 171(2010), No. 1-3, p. 35.

[22] M.Z. Xue and Z.W. Fu, Electrochemical reactions of lithium with transition metal stannides, *Solid State Ionics,* 177(2006), No. 17-18, p. 1501.